LJMU Research Online

Kelvin, LS, Driver, SP, Robotham, ASG, Taylor, EN, Graham, AW, Alpaslan, M, Baldry, IK, Bamford, SP, Bauer, AE, Bland-Hawthorn, J, Brown, MJI, Colless, M, Conselice, CJ, Holwerda, BW, Hopkins, AM, Lara-Lopez, MA, Liske, J, Lopez-Sanchez, AR, Loveday, J, Norberg, P, Phillipps, S, Popescu, CC, Prescott, M, Sansom, AE and Tuffs, RJ

 Galaxy And Mass Assembly (GAMA): stellar mass functions by Hubble type

https://researchonline.ljmu.ac.uk/id/eprint/1509/

Article

For more information please contact researchonline@ljmu.ac.uk

Galaxy And Mass Assembly (GAMA): Stellar mass functions by Hubble type

Lee S. Kelvin,[1,2,3] Simon P. Driver,[2,3] Aaron S. G. Robotham,[3]
Edward N. Taylor,[4] Alister W. Graham,[5] Mehmet Alpaslan,[2] Ivan Baldry,[6]
Steven P. Bamford,[7] Amanda E. Bauer,[8] Joss Bland-Hawthorn,[9]
Michael J. I. Brown,[10] Matthew Colless,[11] Christopher J. Conselice,[7]
Benne W. Holwerda,[12] Andrew M. Hopkins,[8] Maritza A. Lara-López,[8]
Jochen Liske,[13] Ángel R. López-Sánchez,[8,14] Jon Loveday,[15] Peder Norberg,[16]
Steven Phillipps,[17] Cristina C. Popescu,[18] Matthew Prescott,[19]
Anne E. Sansom,[18] and Richard J. Tuffs[20]

[1] *Institut für Astro- und Teilchenphysik, Universität Innsbruck, Technikerstraße 25, 6020 Innsbruck, Austria*
[2] *School of Physics and Astronomy, University of St Andrews, North Haugh, St Andrews, Fife, KY16 9SS, UK*
[3] *International Centre for Radio Astronomy Research, 7 Fairway, The University of Western Australia, Crawley, Perth, Western Australia 6009, Australia*
[4] *School of Physics, the University of Melbourne, Parkville, VIC 3010, Australia*
[5] *Centre for Astrophysics and Supercomputing, Swinburne University of Technology, Hawthorn, Victoria 3122, Australia*
[6] *Astrophysics Research Institute, Liverpool John Moores University, Twelve Quays House, Egerton Wharf, Birkenhead CH41 1LD, UK*
[7] *School of Physics and Astronomy, The University of Nottingham, University Park, Nottingham, NG7 2RD, UK*
[8] *Australian Astronomical Observatory, PO Box 915, North Ryde, NSW 1670, Australia*
[9] *Sydney Institute for Astronomy, School of Physics A28, University of Sydney, NSW 2006, Australia*
[10] *School of Physics, Monash University, Clayton, VIC 3800, Australia*
[11] *Research School of Astronomy and Astrophysics, The Australian National University, Canberra, ACT 2611, Australia*
[12] *European Space Agency, ESTEC, Keplerlaan 1, NL-2200 AG Noordwijk, The Netherlands*
[13] *European Southern Observatory, Karl-Schwarzschild-Str. 2, 85748 Garching, Germany*
[14] *Department of Physics and Astronomy, Macquarie University, NSW 2109, Australia*
[15] *Astronomy Centre, University of Sussex, Falmer, Brighton BN1 9QH, UK*
[16] *Institute for Computational Cosmology, Department of Physics, Durham University, South Road, Durham DH1 3LE, UK*
[17] *Astrophysics Group, H.H. Wills Physics Laboratory, University of Bristol, Tyndall Avenue, Bristol BS8 1TL, UK*
[18] *Jeremiah Horrocks Institute, School of Computing, Engineering and Physical Sciences, University of Central Lancashire, Preston PR1 2HE, UK*
[19] *Astrophysics Group, Department of Physics, University of the Western Cape, 7535 Bellville, Cape Town, South Africa*
[20] *Max Planck Institut für Kernphysik, Saupfercheckweg 1, D-69117 Heidelberg, Germany*

ABSTRACT

We present an estimate of the galaxy stellar mass function and its division by morphological type in the local ($0.025 < z < 0.06$) Universe. Adopting robust morphological classifications as previously presented (Kelvin et al.) for a sample of $3,727$ galaxies taken from the Galaxy And Mass Assembly survey, we define a local volume and stellar mass limited sub-sample of $2,711$ galaxies to a lower stellar mass limit of $\mathcal{M} = 10^{9.0}\mathcal{M}_\odot$. We confirm that the galaxy stellar mass function is well described by a double Schechter function given by $\mathcal{M}^* = 10^{10.64}\mathcal{M}_\odot$, $\alpha_1 = -0.43$, $\phi_1^* = 4.18$ dex^{-1}Mpc^{-3}, $\alpha_2 = -1.50$ and $\phi_2^* = 0.74$ dex^{-1}Mpc^{-3}. The constituent morphological-type stellar mass functions are well sampled above our lower stellar mass limit, excepting the faint little blue spheroid population of galaxies. We find approximately $71^{+3}_{-4}\%$ of the stellar mass in the local Universe is found within spheroid dominated galaxies; ellipticals and S0-Sas. The remaining $29^{+4}_{-3}\%$ falls predominantly within late type disk dominated systems, Sab-Scds and Sd-Irrs. Adopting reasonable bulge-to-total ratios implies that approximately half the stellar mass today resides in spheroidal structures, and half in disk structures. Within this local sample, we find approximate stellar mass proportions for E : S0-Sa : Sab-Scd : Sd-Irr of 34 : 37 : 24 : 5.

Key words: Galaxies – galaxies: elliptical and lenticular, cD – galaxies: spiral – galaxies: luminosity function, mass function – galaxies: fundamental parameters

1 INTRODUCTION

Amongst the veritable cornucopia of observed and derived galaxy parameters, the total stellar mass of a system is arguably one of the most fundamental, perhaps in conjunction with the shape of the galaxy light profile as parameterised by, e.g., the Sérsic (1963) function. One common viewpoint has it that galaxies form via a series of monolithic collapse and/or hierarchical merging events, whereafter evolution continues to occur via additional merging events and stochastic gas accretion phases (e.g., Navarro & Benz 1991; White & Frenk 1991; Cook et al. 2009; L'Huillier et al. 2012; Khochfar & Silk 2006b; De Lucia & Blaizot 2007; Pichon et al. 2011; Wyse et al. 1997; van Dokkum et al. 2010; Khochfar & Silk 2006a; Kormendy & Bender 2012; Kereš et al. 2005; Cook et al. 2010; Debattista et al. 2006). Each stage during this galactic ageing process has an observational impact upon the instantaneous state of a galaxy, e.g.; colour (Baldry et al. 2004, 2008), star formation rate (Behroozi et al. 2013; Moustakas et al. 2013), in addition to leaving a longer term imprint on the nature of the galaxy, e.g.; metallicity (De Lucia et al. 2004; Driver et al. 2013; Lara-López et al. 2013), structure (Cooper et al. 2012; Shankar et al. 2013; Szomoru et al. 2013; Robotham et al. 2013). In many ways this latter parameter, galaxy structure, promises to be the most profound, as rearranging the orbital properties of billions of stars is not a whimsical thing.

Several well known relations between stellar mass and additional complementary galaxy parameters are known to exist, including total size (Graham et al. 2006; Patel et al. 2013), velocity dispersion (Davies et al. 1983; Davies & Illingworth 1983; Shen et al. 2003; Matković & Guzmán 2005), concentration indices and light profile shapes (Caon et al. 1993; Young & Currie 1994; Kauffmann et al. 2003; Blanton et al. 2005; Kelvin et al. 2012), environment (Kauffmann et al. 2004; Baldry et al. 2006), metallicity (Tremonti et al. 2004), metallicity and star formation rate in a 3-dimensional plane (Lara-López et al. 2010) and colour (Conselice 2006). This latter study highlights the importance of stellar mass above other observed parameters, such as star formation rate and merger activity, in describing the maximal variance across the galaxy population. Numerous recent studies explore the division of the local stellar mass budget by, e.g., colour (Baldry et al. 2012; Peng et al. 2012; Taylor et al., 2014, submitted), star formation rate (Pozzetti et al. 2010), environment (Bolzonella et al. 2010) and coarse morphology (Bundy et al. 2010). Here we study the relation between stellar mass and morphology, specifically; how the local galaxy stellar mass function (GSMF) is built from different morphological types. A standard cosmology of $(H_0, \Omega_m, \Omega_\Lambda)$=(70 km s^{-1} Mpc^{-1}, 0.3, 0.7) is assumed throughout this paper.

2 DATA

Our data is taken from the Galaxy And Mass Assembly survey (GAMA: Driver et al. 2009, 2011) phase 1 (GAMA I). GAMA is a combined spectroscopic and multi-wavelength imaging survey designed to study spatial structure in the nearby ($z < 0.25$) Universe on scales of 1 kpc to 1 Mpc. The GAMA regions lie within areas of sky previously surveyed by both SDSS (York et al. 2000; Abazajian et al. 2009) as part of its Main Survey, and UKIRT as part of the UKIDSS Large Area Survey (UKIDSS-LAS; Lawrence et al. 2007).

Using the latest version (version 16) of the GAMA I tiling catalogue[1] (*TilingCatv16*, see Baldry et al. 2010), we adopt a local, volume and luminosity limited sample of 3,727 galaxy-like (SURVEY_CLASS $\geqslant$ 2) objects, GAMAnear, previously defined in Kelvin et al. (2014). In brief, this sample is defined thus:

- a local flow-corrected spectroscopic redshift z of $0.025 < z < 0.06$ with an associated GAMA redshift quality flag of $nQ > 2$ (i.e., good for science),
- a Milky Way dust extinction corrected apparent r band SDSS (DR7) Petrosian magnitude of $r < 19.4$ mag,
- an absolute Sérsic magnitude truncated at 10 multiples of the half-light radius in the r-band of $M_r < -17.4$ mag.

Local flow-corrected spectroscopic redshifts are taken from the GAMA I *DistancesFramesv07* catalogue (Baldry et al. 2012). For this sample, we adopt an upper redshift limit of $z = 0.06$. This limit is chosen such that the majority of bulges (the limiting structural component) should remain resolvable[2]. To calculate this limit, typical bulge half-light radii for galaxies in the local Universe are estimated based on prior bulge-disk decompositions presented in Allen et al. 2006 (~ 1.93 kpc) and Simard et al. 2011 (~ 3.02 kpc, see Kelvin et al. 2014 for a complete discussion). Our upper redshift limit is determined using these data to estimate the maximal redshift out to which a bulge would remain larger than the average seeing found in SDSS imaging ($\sim 1.1''$, see Kelvin et al. 2012). At $z = 0.06$, $1.1''$ corresponds to a physical size of 1.28 kpc. Therefore, bulge half-light diameters are at least three times the median r band seeing at $z = 0.06$. A lower limit of $z = 0.025$ is also adopted to avoid low galaxy number densities below this redshift and such that redshifts are not dominated by peculiar velocities. (see Kelvin et al. 2014 for further details). Our redshift limits give this sample a volume of 2.1×10^5 Mpc^3. Matching the GAMAnear sample to the GAMA galaxy group catalogue (G3C; Robotham et al. 2011), we find that just under half (1797, $\sim 48\%$) of our galaxies lie in identified groups, with a median halo mass of $\mathcal{M}_H \sim 10^{12.9} \mathcal{M}_\odot$. Of these galaxies, 672 ($\sim 18\%$) lie in groups with a richness greater than 5, with a median halo mass of $\mathcal{M}_H \sim 10^{13.5} \mathcal{M}_\odot$. Owing to this, our sample should be considered predominantly field dominated, extending into the intermediate-mass group regime.

Our SDSS DR7 (York et al. 2000; Abazajian et al. 2009) apparent Petrosian magnitude limit of $r = 19.4$ is chosen to correspond to the main GAMA I spectroscopic target selection limit (Driver et al. 2009; Baldry et al. 2010), ensuring completeness across all three equatorial GAMA regions[3].

---

[1] All data release 2 GAMA catalogues are available through the GAMA database, available online at http://www.gama-survey.org/dr2/ .

[2] Assuming of course a sufficiently high B/T ratio which allows for the detection of bulge flux above the host disk flux.

[3] Whilst the central 12h equatorial GAMA field (G12) reaches a greater limiting depth of $r = 19.8$, we choose not to consider this extra data here to maintain a consistent depth of $r = 19.4$ across all three primary GAMA fields.

Sérsic magnitudes are robustly derived using the galaxy 2D light-profile modelling package SIGMA (Kelvin et al. 2010, 2012). Information on their derivation, and a further discussion of our choice to truncate these extrapolated light-profile fits to 10 multiples of the half light radius may be found in Kelvin et al. (2012). Our absolute Sérsic magnitude r-band limit of $M_r < -17.4$ mag is chosen to avoid the effects of Malmquist bias out to our upper redshift limit of $z = 0.06$. A further discussion of this limit can be found in Kelvin et al. (2014).

The GAMAnear dataset is visually morphologically classified in Kelvin et al. (2014) by three independent observers into their appropriate Hubble type, namely; elliptical (E), lenticular/early-type spiral (S0-Sa, barred and unbarred), intermediate/late-type spiral (Sab-Scd, barred and unbarred), disk-dominated spiral or irregular (Sd-Irr), star (see below) and little blue spheroid (LBS). Classifications are assigned on a majority agreement basis; at least two of the three observers must agree on the classification. In the result of a three-way tie (only occurring for 56 galaxies, or 1.5% of the total sample), preference is given to the senior observer.

As previously noted in Kelvin et al. (2014), the LBS type galaxy is typically compact, spheroidal and blue, hence their designation as 'Little Blue Spheroids'. The median colour of LBS galaxies within our GAMAnear sample is $g - i \sim 0.6$ with a median Sérsic index of $n_r \sim 1.9$ in the r band ($n_K \sim 1.6$ in the K band) and a median physical size of $r_e \sim 1.1$ kpc in the r band ($r_e \sim 0.9$ kpc in the K band). Because of their physical similarities with both spheroids and disks, it is not immediately apparent which structural class these objects should be associated with. For a further discussion of our LBS class, we refer the reader to Kelvin et al. (2014), and we note that a dedicated study is currently in progress in order to better understand our LBS population (Moffett et al., in prep.).

We acknowledge the apparent difficulty in visually dividing galaxies along the elliptical/lenticular interface, as highlighted in the recent literature, e.g., Bamford et al. (2009); Emsellem et al. (2011); Cappellari et al. (2011a, 2013). A face on lenticular galaxy may appear, even to the expert classifier, as a smooth 1-component system, and therefore be mis-classified as an elliptical galaxy. As a consequence of this, the S0-Sa class will suffer from a shortfall in the correct number of S0 type galaxies. Nevertheless, in keeping with the classification methodology of our original study (Kelvin et al. 2014), here we opt to maintain this division between elliptical and lenticular type galaxies.

The latter 'star' type refers to incorrectly targeted foreground stars in front of a background galaxy (to which the associated redshift belongs) or segments of a large diffuse galaxy, and therefore this population shall be discarded from subsequent morphological analyses. Owing to low number statistics for our barred systems, the barred populations have been merged into their sibling unbarred classes. Any subsequent discussion of the barred populations alone are provided for completeness sake, in keeping with the classification criteria established in Kelvin et al. (2014), but this information is not used for scientific analyses. For further details on our morphological dataset and base sample selection criteria, see Kelvin et al. (2014).

2.1 Stellar Masses

Stellar masses used in this study are taken from version 8 of the GAMA I stellar mass catalogue (*StellarMassesv08*; Taylor et al. 2011). In summary, a series of Bruzual & Charlot (2003) composite stellar population spectral models are created, adopting a Chabrier (2003) Initial Mass Function and using a Calzetti et al. (2000) dust attenuation law. A stellar population library is constructed under the assumptions of a single metallicity and a continuous exponentially declining star formation history for each stellar population. Dust is modelled as a single uniform screen. These spectra are subsequently rescaled by some normalisation factor in order that the synthetic spectral flux matches that as defined by a series of Kron-like (AUTO) apertures as detailed in Hill et al. (2011). The value of the normalisation factor determines the AUTO aperture defined stellar mass for that particular system, $\mathcal{M}_{*,\mathrm{AUTO}}$.

We apply a secondary Sérsic flux correction to the AUTO defined stellar masses as recommended in Taylor et al. (2011). As shown in Graham & Driver (2005), both Petrosian and Kron-like photometry have the potential to miss flux in the wings of large, extended systems (particularly those with high Sérsic indices). Sérsic photometry is ideally suited to correct for this effect, and so we choose to apply it to these data. Our final stellar mass estimates, $\log\left(\frac{\mathcal{M}_*}{\mathcal{M}_\odot}\right)$, are given using the equation

$$\log\left(\frac{\mathcal{M}_*}{\mathcal{M}_\odot}\right) = \log\left(\frac{\mathcal{M}_{*,\mathrm{AUTO}}}{\mathcal{M}_\odot}\right) + \log\left(\frac{L_{\mathrm{Sérsic}}}{L_{\mathrm{AUTO}}}\right) \qquad (1)$$

where L_{AUTO} and $L_{Sérsic}$ are the (linear) r-band AUTO aperture flux and the total r-band flux inferred from fitting a Sérsic profile truncated at 10 multiples of the half-light radius (as given in Kelvin et al. 2012), respectively. The scale factor $L_{\mathrm{Sérsic}}/L_{\mathrm{AUTO}}$ describes the additional flux given by our single Sérsic model fits relative to the standard GAMA AUTO photometry. For each morphological type we find the following median Sérsic–AUTO flux scale factors; LBS=1.01, E=1.03, S0-Sa=1.05, Sab-Scd=1.01, Sd-Irr=1.00. Note that our resultant stellar mass estimates refer to the stellar mass implied via the visible flux from the living stellar population within a galaxy, and not the total living plus faint/dark remnant (i.e., white dwarf, neutron star, black hole, etc.) populations (Shimizu & Inoue 2013).

As expanded upon in Baldry et al. (2012), the GAMAnear sample will suffer from surface brightness limitations at the faint/low-mass end of our sample owing to photometric incompleteness. Figure 11 of Baldry et al. (2012) shows the relation between surface brightness and stellar mass for a subset of the GAMA dataset across a similar redshift range. Clearly, the impact of surface brightness incompleteness becomes increasingly severe in the mass range $\log(\mathcal{M}_*/\mathcal{M}_\odot) = 8.0 - 9.0$. To mitigate the effects of incompleteness, we adopt the extreme of this range and that recommended in Baldry et al. (2012), $\log(\mathcal{M}_*/\mathcal{M}_\odot) = 9.0$, as an additional stellar mass limit to our sample. This reduces our GAMAnear sample from $3,727$ galaxies to $2,711$ (73% of the GAMAnear dataset).

The well-established relation between colour and mass-to-light ratio (e.g., Figure 12, Taylor et al. 2011) implies that galaxies with a higher mass-to-light ratio tend towards be-

ing redder in colour. Therefore, for a given luminosity, redder galaxies appear more massive than their bluer counterparts. Consequently, for galaxies in our volume and r band magnitude limited GAMAnear sample, at a given stellar mass, one is able to see bluer galaxies out to a higher redshift than red systems (e.g., Figure A1, van den Bosch et al. 2008). Alternatively, at a given redshift, the stellar mass completeness limit is higher for red galaxies than for blue. In order to fully account for any potential incompleteness bias within our remaining mass-limited sample of 2, 711 galaxies, we also opt to weight each galaxy above our mass limit according to $W = V_{tot}/V_{max}$ (Schmidt 1968); the ratio of the total observed volume (2.1×10^5 Mpc^3) to the maximum comoving volume over which the galaxy could have been observed within the survey limits. The corresponding z_{max} is the maximum redshift at which a galaxy can be seen based on its spectral shape and survey limits ($r = 19.4$ mag). We adopt z_{max} values as presented in Taylor et al. (2011) and available in the GAMA StellarMassesv08 catalogue in order to calculate V_{max} estimates. Weights in the range $W < 1$, i.e., $V_{tot} < V_{max}$, are set equal to 1. All stellar masses presented hereafter should be assumed to have this V_{max} weight correction applied, unless otherwise stated.

This volume and stellar mass limited sample of 2, 711 galaxies, GAMAnear$\mathcal{M}_{lim}$, constitutes our primary dataset, and shall be used throughout the remainder of this paper. Both GAMAnear and GAMAnear$\mathcal{M}_{lim}$ are shown in redshift–stellar mass space in Figure 1.

3   STELLAR MASS AND MORPHOLOGY

Figure 2 shows the stellar mass breakdown by type and morphology for the entirety of our mass limited sample of 2, 711 galaxies. Within each classification bubble, values for the logarithm of the median stellar mass (left) and the percentage by stellar mass with associated error (right) are shown. Percentage by stellar mass is calculated via a simple summation of the V_{max}-weighted stellar mass of each galaxy within each population. Percentage errors represent the maximal dispersion between the three independent classifiers, i.e., the stellar mass for each galaxy population is rederived for each classifier and the offset from the master classification calculated. Note that the stellar masses for each galaxy as derived in Taylor et al. (2011) have a typical associated intrinsic stellar mass error of $\Delta \log{(\mathcal{M}_*/\mathcal{M}_\odot)} \sim 0.1$.

Approximately $71^{+3}_{-4}\%$ of the stellar mass in our GAMAnear$\mathcal{M}_{lim}$ sample is currently found within spheroid dominated[4] (elliptical and S0-Sa) systems, with the remaining stellar mass in disk dominated (Sab-Scd and Sd-Irr) galaxies ($29^{+4}_{-3}\%$) and little blue spheroids ($\sim 0.52\%^{+0.3}_{-0.2}$).

---

[4] Here, the term 'spheroid dominated' does not refer to the spheroidal component dominating the total flux of the system. As has been shown in Graham & Worley (2008), rarely does the spheroid component in a bulge+disk system contribute $> 50\%$ of the flux for galaxies later than S0. Rather, we define the term 'spheroid dominated' to refer to the visual impact of the spheroid on the postage stamp images presented in Kelvin et al. (2014); a combination of relative size, apparent surface brightness and 2D light profile.
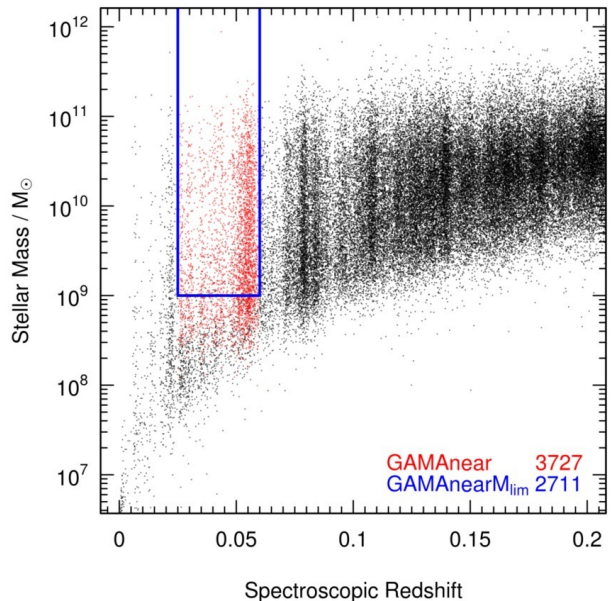

Figure 1. Stellar mass as a function of redshift for galaxies within the GAMA survey. The red data points represent our GAMAnear sample; those galaxies that lie in the redshift range $0.025 < z < 0.06$ with an associated GAMA redshift quality flag of $nQ > 2$ (i.e., good for science), an extinction corrected r band SDSS Petrosian magnitude of $r < 19.4$ mag and an absolute truncated Sérsic magnitude in the r-band of $M_r < -17.4$ mag. GAMAnear galaxies that additionally are more massive than $\log{(\mathcal{M}_*/\mathcal{M}_\odot)} > 9.0$ (within the blue box) constitute our stellar mass limited sample, GAMAnearM$_{lim}$, in use throughout the remainder of this paper. Stellar masses shown here are not V_{max} weight corrected.

Adopting reasonable bulge-to-total values (e.g., for an intermediate Sb spiral, $\log{(B/D)} \sim -1$, Graham & Worley 2008) implies that approximately half the stellar mass today resides in spheroidal structures[5], with the remaining half within disk-like structures, in-line with previous studies (see Driver et al. 2007a,b; Gadotti 2009; Tasca & White 2011). Continuing further down the classification tree, we find approximate stellar mass proportions for E : S0-Sa : Sab-Scd : Sd-Irr of 34 : 37 : 24 : 5. For comparison, table 1 shows the number fractions of various galaxy populations in stellar mass ranges with progressively more massive lower bounds. We see that no LBS type galaxies exist in the mass range $\log{(\mathcal{M}_*/\mathcal{M}_\odot)} > 10.0$. Spheroid dominated galaxies become more numerous than disk dominated galaxies at $\log{(\mathcal{M}_*/\mathcal{M}_\odot)} > 9.5$, whilst elliptical galaxies alone dominate the galaxy population by number at $\log{(\mathcal{M}_*/\mathcal{M}_\odot)} > 11.0$. Interestingly, at stellar masses less massive than $\log{(\mathcal{M}_*/\mathcal{M}_\odot)} = 11.0$, $\sim 25\%$ of the total galaxy population are consistently elliptical.

Our elliptical stellar mass fraction of $34\%^{+9}_{-4}$ is in excellent agreement with the value of 32% found in Gadotti (2009)[6] but significantly higher than the $\sim 15\%$ value found

---

[5] One expects the bulge-to-total ratio to correlate with the total stellar mass of the system, and therefore, this value should be considered an estimate.

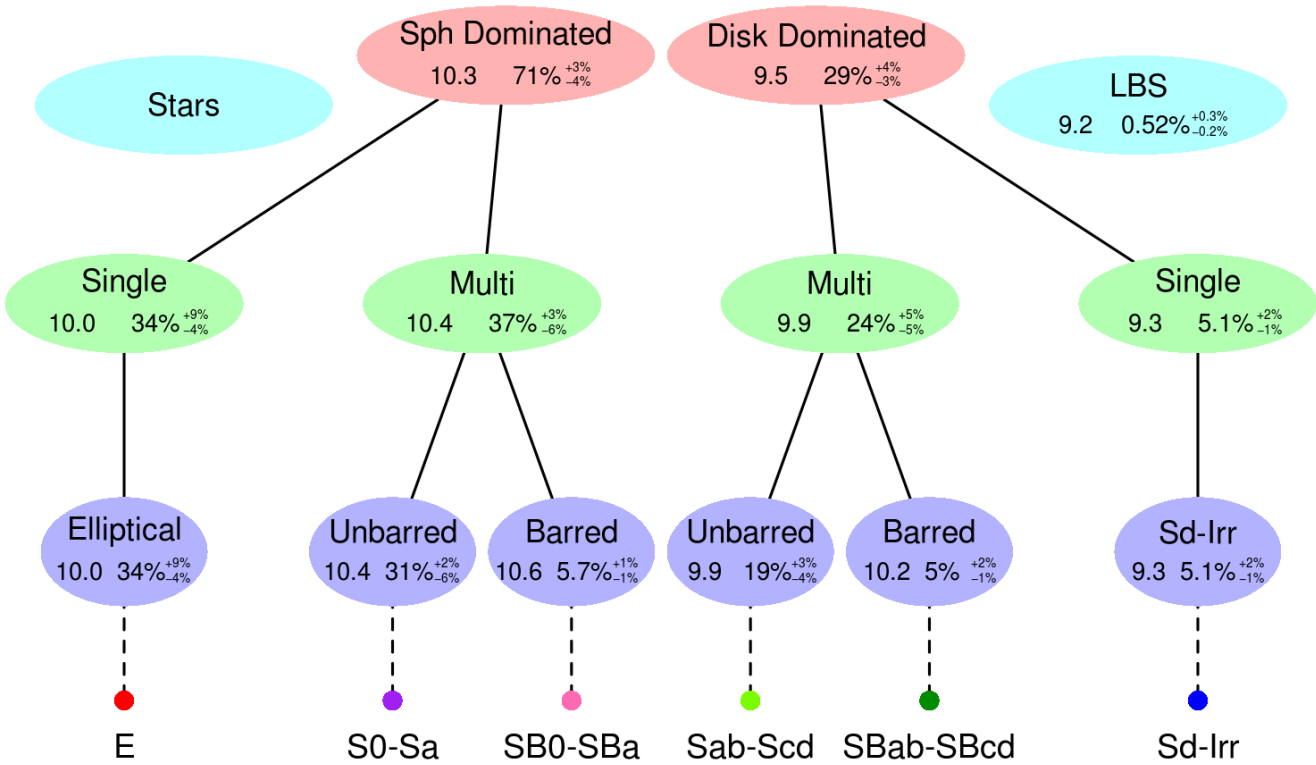[6] Note that whilst the sample in Gadotti 2009 spans a similar

Figure 2. The breakdown of stellar mass within our GAMAnear$\mathcal{M}_{\mathrm{lim}}$ sample by morphological type. Within each classification bubble, values for the logarithm of the median stellar mass (left) and the percentage of total stellar mass with its associated error (right) are shown. Stellar masses shown here have been V_{max} weight corrected.

Population	Stellar Mass Range $[\log(\mathcal{M}_*/\mathcal{M}_\odot)]$					
	> 9	> 9.5	> 10	> 10.5	> 11	> 11.5
LBS	0.04	0.01	0.00	0.00	0.00	0.00
E	0.19	0.24	0.24	0.31	0.72	1.00
S0-Sa	0.18	0.28	0.42	0.48	0.22	0.00
Sab-Scd	0.28	0.36	0.32	0.20	0.06	0.00
Sd-Irr	0.31	0.11	0.02	0.00	0.00	0.00
Sph Dom	0.37	0.51	0.66	0.80	0.94	1.00
Disk Dom	0.59	0.47	0.34	0.20	0.06	0.00

Table 1. The number fractions of various galaxy populations for stellar mass ranges with progressively more massive lower bounds, as indicated. Barred populations have been merged into their sibling unbarred classes. Stellar masses shown here have been V_{max} weight corrected.

in Driver et al. (2007a). This presumably reflects the great difficulty in distinguishing between genuine pressure supported ellipticals and rotationally supported face-on lenticulars, as highlighted by the ATLAS3D team, see for example

redshift range, their lower stellar mass limit is 1 dex higher, 10^{10} $\mathcal{M}_\odot$, than that adopted here.

Emsellem et al. (2011); Krajnović et al. (2011); Cappellari et al. (2011b); Duc et al. (2011); Khochfar et al. (2011), also D'Onofrio et al. (1995); Graham et al. (1998). If the Driver et al. study is correct then the potential contamination of our elliptical class by lenticular types may be significant. A key difference in our classifications and that of Driver et al. is the method of selection, with the former using eyeball morphology based on SDSS/UKIDSS data and the latter using GIM2D bulge-disc decompositions based on the significantly deeper Millennium Galaxy Catalogue *B* band data (see Liske et al. 2003; Driver et al. 2005). The Gadotti (2009) elliptical class is based on a Petrosian concentration index cut. In Driver et al. (2006) it was reported than the E/S0 (red spheroid) class contains $(35 \pm 2)\%$ of the stellar mass, which is closer to our elliptical value, and perhaps supporting the notion that our visually classified E class potentially contains a large fraction of lenticular contaminants. We will explore this issue in detail using robust structural decompositions (Kelvin et al., in prep.) based on the GALFIT galaxy fitting software (Peng et al. 2002, 2010a) and via ongoing SAMI and CALIFA integral field unit observations (in progress). At present we advocate a small amount of caution in regards to the level of potential lenticular contamination of our elliptical sample.

4   THE STELLAR MASS FUNCTION

4.1   The Galaxy Stellar Mass Function

One of the most fundamental measurements in astronomy is that of the galaxy luminosity function, or its equivalent in mass, the galaxy stellar mass function (hereafter GSMF). The GSMF gives the effective number of galaxies per unit volume in the logarithmic stellar mass interval $\log \mathcal{M}$ to $\log \mathcal{M} + d \log \mathcal{M}$, where $d \log \mathcal{M}$ is some log base 10 mass interval. Adopting the GAMA stellar masses presented in Taylor et al. (2011), we calculate our GSMF (and also our MSMFs below) via a direct summation of stellar mass in bins of 0.1 dex.

The GSMF may be described using a Schechter (1976) function whereby the number density, $\Phi (\log \mathcal{M}) \, d \log \mathcal{M}$, is given by

$$
\begin{aligned}
\Phi (\log \mathcal{M}) \, d \log \mathcal{M} \quad = \quad & \ln(10) \cdot \phi^* 10^{\log(\mathcal{M}/\mathcal{M}^*)(\alpha+1)} \\
& \times \exp \left(-10^{\log(\mathcal{M}/\mathcal{M}^*)} \right) d \log \mathcal{M} \, (2)
\end{aligned}
$$

where $\mathcal{M}^*$ is the characteristic mass corresponding to the position of the distinctive 'knee' in the mass function. The terms α and ϕ^* refer to the slope of the mass function at the low mass end and the normalisation constant, respectively. Several recent studies have previously measured the GSMF (e.g.; Baldry et al. 2008; Peng et al. 2010b; Baldry et al. 2012), and advocate the double Schechter form of the GSMF with a combined knee ($\mathcal{M}^*$) for the global population. The double Schechter function is simply given by $\Phi_{double} (\log \mathcal{M}) \, d \log \mathcal{M} = \Phi_1 + \Phi_2$, where Φ_1 and Φ_2 refer to Equation 2 above, albeit with separate slope parameters, α_1 and α_2, and unique normalisation values, ϕ_1^* and ϕ_2^*. Both Φ_1 and Φ_2 share a common $\mathcal{M}^*$ parameter. The double Schechter function allows one to more accurately model the distinctive bump observed in the GSMF about $\mathcal{M}^*$, with one Schechter function dominant at stellar masses greater than $\mathcal{M}^*$, and the second dominant otherwise. We adopt this technique, opting to fit the GSMF with a double Schechter model[7], however, we maintain a single Schechter model for the morphological-type stellar mass functions (MSMFs hereafter) that constitute it.

4.2   Morphological-Type Stellar Mass Functions

Figure 3 shows our GSMF and constituent MSMFs for our volume and stellar mass limited GAMAnear$\mathcal{M}_{\text{lim}}$ sample of $2,711$ systems. Stellar masses shown here have been V_{max} weight corrected where appropriate. The solid black line indicates a double Schechter fit to the total GSMF, binned into mass bins of 0.1 dex, whilst the various orange lines show similar GSMF double Schechter fits found in recent studies (Baldry et al. 2008; Peng et al. 2010b; Baldry et al. 2012; Peng et al. 2012). Note that we choose not to match to

---

[7] All Schechter functions are fit using the NLMINB routine in R; a quasi-Newton algorithm based on the PORT routines that optimise fitting in a similar sense to the Limited-memory Broyden-Fletcher-Goldfarb-Shanno algorithm (LM-BFGS), with an extension to handle simple box constraints on input variables (L-BFGS-B). The PORT documentation is available at http://netlib.bell-labs.com/cm/cs/cstr/153.pdf

additional complementary studies, such as that of Taylor et al. (2014, submitted) which divides their sample into statistically defined 'R' and 'B' populations, or the older yet still equally valid studies of Bell et al. (2003) and Baldry et al. (2004). This is for the sake of clarity alone, to avoid confusion within our Figure 3. Solid coloured lines indicate single Schechter fits to the constituent MSMFs, where colour relates to morphology as indicated by the inset legend. Note that no Schechter fit to the LBS population is shown, as there was not sufficient data to constrain a Schechter function at this low mass end of the dataset. Shaded grey areas ($\log (\mathcal{M}_*/\mathcal{M}_\odot) < 9.0$ and number of galaxies $n \leqslant 3$) indicate those regions where data has not been used in constraining the Schechter fits. Data points below our lower mass limit are from the parent GAMAnear sample, and are shown only for reference. Also consider that the GAMA dataset exhibits a high level of spectroscopic completeness ($> 98\%$) down to its stated limiting apparent magnitude depth of $r = 19.4$ mag (Driver et al. 2011), which precludes the possibility of severely impacting our measured stellar mass functions. The upper panel of Figure 3 shows the number fraction of galaxies as a function of V_{max} weight corrected stellar mass, calculated in mass bins identical to those in the lower panel. Shaded coloured regions around each morphological-type fraction line within the upper panel indicate the $\pm 1\sigma$ confidence intervals, as calculated using the QBETA function (Cameron 2011).

We find our global GSMF in excellent agreement with the complementary studies shown in Figure 3, exhibiting a comparable $\mathcal{M}^*$ Schechter fit parameter at $\log (\mathcal{M}^*/\mathcal{M}_\odot) = 10.64 \pm 0.07$, and agreeing well within the errors. The high mass end of our sample predominantly consists of spheroid dominated elliptical and S0-Sa type galaxies. At intermediate masses below the global $\mathcal{M}^*$ value, the disk dominated Sab-Scd population dominates the stellar mass budget, whilst at the low mass end of our dataset the Sd-Irr and LBS populations are the most influential. It is apparent that the latter LBS population is poorly sampled in this mass regime, with the $\mathcal{M}^*$ parameter likely residing below our lower stellar mass limit of $\log (\mathcal{M}_*/\mathcal{M}_\odot) = 9.0$. For this reason, we do not provide Schechter function fit parameters to the LBS population in this study. We remind the reader that this sample should be considered a field dominated sample, rather than a cluster environment, as is evidenced by the dominance of Sd-Irr and LBS type systems at the low mass end of our dataset.

Because of the uncertainty in our elliptical/S0-Sa division, and in an attempt to group galaxies into structurally meaningful parent samples, we now also combine our morphological types into two populations in Figure 4 as indicated, namely: spheroid dominated (E, S0-Sa) and disk dominated (Sab-Scd, Sd-Irr) galaxies, and similarly fit these data with a single Schechter function. our recovered $\mathcal{M}^*$ Schechter fit parameters for our combined stellar mass functions are remarkably similar to one another and to our total GSMF, with $\log (\mathcal{M}^*/\mathcal{M}_\odot) = 10.60$ and 10.70, respectively, supporting the notion that the combined total galaxy stellar mass function is well described by a double Schechter function comprised of two distinct components identified morphologically here. Comparison Schechter function fits for a similar red and blue population from Baldry et al. (2012) and Peng et al. (2012) are also shown in Figure 4. The
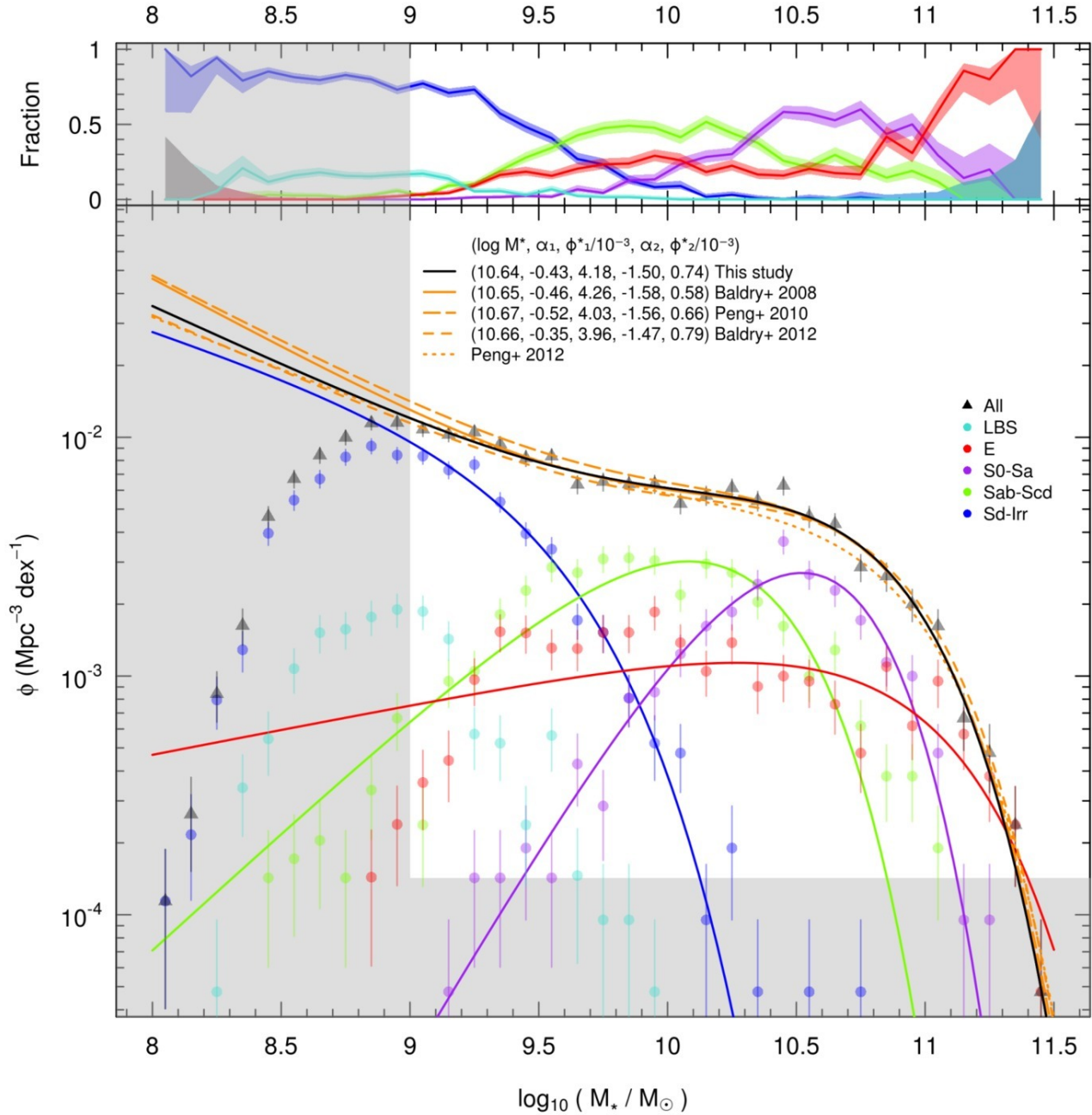
Figure 3. The Galaxy Stellar Mass Function and constituent Morphological-Type Stellar Mass Functions as fit by double and single Schechter functions respectively. Each galaxy population is labelled and coloured according to the inset legend. The data is split into mass bins of 0.1 dex, with the error per bin assumed to be Poissonian ($\sqrt{n}$) in nature. Shaded grey areas ($\log\,(\mathcal{M}_*/\mathcal{M}_\odot) < 9.0$ and number of galaxies $n \leqslant 3$) indicate those regions where data has not been used in constraining the Schechter fits. Schechter fit parameters for the GSMF in addition to fits from other studies are also shown for reference. The upper panel shows the number fraction of galaxies as a function of V_{max} weight corrected stellar mass, calculated in mass bins identical to those in the lower panel. Shaded coloured regions around each morphological-type fraction line indicate the $\pm 1\sigma$ confidence intervals, as calculated using the QBETA function (Cameron 2011).

Peng et al. GSMF is a summation of Schechter function fits to red/blue central and red/blue satellite galaxies. We find our disk dominated population in excellent agreement with the Baldry et al. and Peng et al. blue populations, agreeing well at the lowest stellar masses, whilst we find a slight surplus of stellar mass in disk dominated galaxies at masses

greater than $\mathcal{M}^*$. Our spheroid dominated population similarly shows a good level of agreement at the most massive end of our sample beyond $\mathcal{M}^*$, however; we do not find the low mass turn up found in the comparison red populations.

The cause of this discrepancy remains somewhat a mystery, and perhaps rests with our choice of comparison
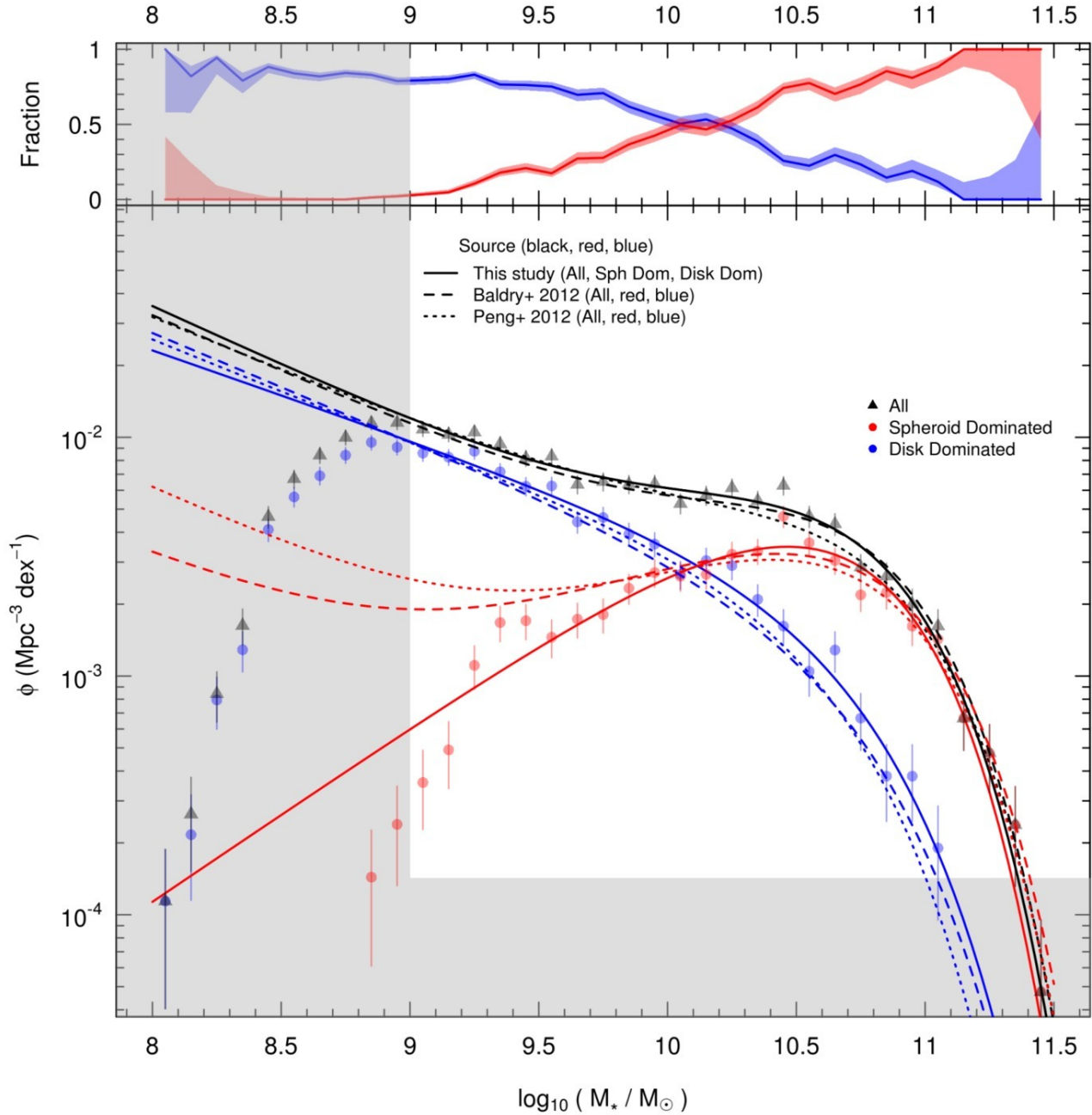
Figure 4. As Figure 3, but for a reduced grouping of morphological types, as indicated, which may broadly be compared to early type and late type galaxies. Comparison Schechter function fits for similar red and blue populations from Baldry et al. (2012) and Peng et al. (2012) are also shown.

samples. For example, Yang et al. (2009) find no low-mass turn up for their red population across a stellar mass regime comparable to that probed here, disagreeing with the studies above, and highlighting apparent difficulties when dividing the galaxy population by colour alone. Similarly, whilst Muzzin et al. (2013) and Tomczak et al. (2014) do find a low-mass turn up in the stellar mass function of quiescent galaxies when dividing the galaxy population into quiescent/star-forming sub-populations, Omand et al. (2014) find no noticeable low-mass turn up for their equivalent quiescent sample.

To expand on the relation between colour and stellar mass, Figure 5 shows global rest frame colour, $(g - i)_{\rm rest}$, as a function of galaxy stellar mass, $\log{(\mathcal{M}_*/\mathcal{M}_\odot)}$. Our rest-frame colours are those derived concurrently with the stellar masses from Taylor et al. (2011), i.e., an SED fit to the GAMA galaxy photometry. The top left panel displays several overlaid contour maps highlighting the population density in colour-mass space for all of our morphological types, as indicated by the inset legend, whereas the remaining panels represent the same colour-mass space for each popula-

tion in isolation, as labelled in the top left corner of each panel. For these latter panels, we display a 3-colour (RGB = Hig)[8] postage stamp image of a galaxy at each position within a grid of bin size 0.1 in stellar mass and 0.03 in colour, where a blank space indicates no galaxy of that morphological type exists. In total in this figure, we display $1,245$ galaxies from our GAMAnear sample (32.5%), with each postage stamp approximately $7'' \times 7''$ in size. We find the spheroid dominated elliptical and lenticular/early type red sequence extending across a wide range of stellar masses, $9.5 < \log(\mathcal{M}_*/\mathcal{M}_\odot) < 11.5$ with a relatively small variation in global $(g-i)_{\rm rest}$ colour across this range. As can also be seen in Figure 3, the elliptical population rarely dominates the stellar mass budget in this range for any given stellar mass, except at the most massive extreme of our sample ($\log(\mathcal{M}_*/\mathcal{M}_\odot) \sim 11$). At stellar masses below $\log(\mathcal{M}_*/\mathcal{M}_\odot) \approx 10.2$, first the disk dominated Sab-Scd population followed by the Sd-Irr population provide a significant contamination fraction to the red sequence. This contamination 'break-point' is in good agreement with that reported in Taylor et al. (2014, submitted), whereby the mean colour of a statistically defined red population of galaxies jumps by ≈ 0.2 mag, coupled with an increase in scatter, at $\log(\mathcal{M}_*/\mathcal{M}_\odot) \approx 10.1$.

One possible explanation behind this red sequence contamination becomes apparent in the postage stamps for the Sab-Scd and Sd-Irr population panels. In the colour regime $(g-i)_{\rm rest} > 0.7$, a significant fraction of disk dominated galaxies are observed highly inclined or edge on. The reprocessing of galactic light as it travels through a disk has the effect of reddening the resultant light due to the effects of intrinsic dust attenuation, so therefore any photometric estimate of the global colour will be biased redwards, in addition to affecting other measured photometric properties (e.g.; Pastrav et al. 2013). This late type morphological contamination of the red sequence, effectively a redistribution of stellar mass from the blue to the red population, may perhaps be responsible for the observed turn up of the red population stellar mass functions at the low mass end reported in, e.g., Baldry et al. (2012); Peng et al. (2012). Further, we posit that any such division of the local galaxy population by (uncorrected) colour into a red sequence and blue cloud, such as that adopted by, e.g., Bell et al. 2003; Baldry et al. 2004 (a division in colour-magnitude space) and Peng et al. 2010b (a division in colour-stellar mass space), becomes increasingly meaningless at stellar masses below $\log(\mathcal{M}_*/\mathcal{M}_\odot) \approx 10.2$.

We stress however that colour is no more equivalent to spheroid/disk-dominated than it is to quiescent/star-forming, slow/fast rotator, early-type/late-type or metal rich/poor, to name but a few common bimodal galaxy identities. Whilst significant overlaps may, and do, exist between these populations, they do in fact measure distinct galaxy populations, and therefore one may not always expect to recover a similar trend in, for example, the observed stellar mass function. Also consider that our choice to construct a

spheroid-dominated sample from elliptical and S0-Sa galaxies alone undoubtedly influences our recovered stellar mass functions. We note that, should we choose to include the LBS population into the spheroid-dominated population, we similarly recover a low-mass turn up such as that observed in Baldry et al. (2012) and Peng et al. (2012). However, since LBS galaxies are notably blue, one might expect any division by colour to bin LBS galaxies with our typically blue disk-dominated systems, increasing the number density for the disk-dominated population alone, and therefore not providing the required turn-up for spheroid-dominated systems in the low mass regime. See Appendix A for a further discussion of the inclusion of the LBS population into our spheroid dominated class.

Full Schechter fit parameters for both the double GSMF and constituent MSMFs (both Hubble type morphologies and combined spheroid/disk dominated populations) are shown in Tables 2 and 3 respectively. As previously noted, we do not provide Schechter fit parameters for the LBS population. Errors on the ρ_Σ parameter are propagated through from the stellar mass errors estimated in Taylor et al. (2011), typically of the order ~ 0.1 dex. The second set of errors for the $\log\mathcal{M}^*$, α and ϕ^* parameters represent one standard deviation as derived from comparable Schechter function fits to each individual observers data set alone, giving an indication of classification agreement between all three observers. All other errors provided in both tables are estimated from jackknifed resampling using the relation $\sigma^2 = \frac{N-1}{N}\sum_{i=1}^{N}(x_j - x)^2$, where x is the best fit parameter, x_j is the best fit parameter as given from a jackknife resampled variant of the data set and N represents the number of jackknife volumes (we adopt $N = 10$).

The double Schechter GSMF provides a good fit to the bimodal form of the total population, with a goodness of fit parameter of $\chi^2/\nu = 1.12$ (a χ^2 p-value of $p = 0.33$, with $\chi^2 = 21.2$ and $k = 19$ degrees of freedom; i.e., we have insufficient evidence to reject our fitted model). As can be inferred from Figure 3 and the gradient of the elliptical population in Table 3, the initial high-mass peak primarily consists of S0-Sa galaxies, with some small contribution from elliptical galaxies. Ellipticals appear to exist uniformly across a wide range of masses. Our fitted Schechter function to the elliptical population appears to be a relatively poor fit to the data, as evidenced by the goodness of fit parameter and confidence intervals quoted in Table 3, able to capture the high mass turnover about $\mathcal{M}^*$ but partially underestimating the number counts at lower stellar masses. No doubt this discrepancy is caused by the inflexibility of the Schechter function in fitting a population that is uniformly distributed in number density such as this. Similarly, the goodness of fit parameter for the Sab-Scd population is quite poor. From Figure 3 we see that this discrepancy occurs at the high mass end, above $\mathcal{M}^*$, with an unexpected surplus of galaxies and a departure from the Schechter fit at $\log(\mathcal{M}^*/\mathcal{M}_\odot) \sim 11$. This could be evidence of perhaps spheroid dominated (elliptical, lenticular or early-type spiral) contamination of the Sab-Scd population in this regime. In addition, errors arising from observer disagreement place a significant level of uncertainty on Schechter fit parameters to our Sd-Irr population. This implies that perhaps these data are not of a sufficient depth to fully measure the characteristic turn-over in the Sd-Irr stellar mass function.

---

[8] Postage stamps of a peculiar turquoise colour indicate galaxies that lie in a region where no near-infrared (UKIDSS-LAS) data was available at the time of postage stamp creation, hence a missing red channel in the creation of our 3-colour images.
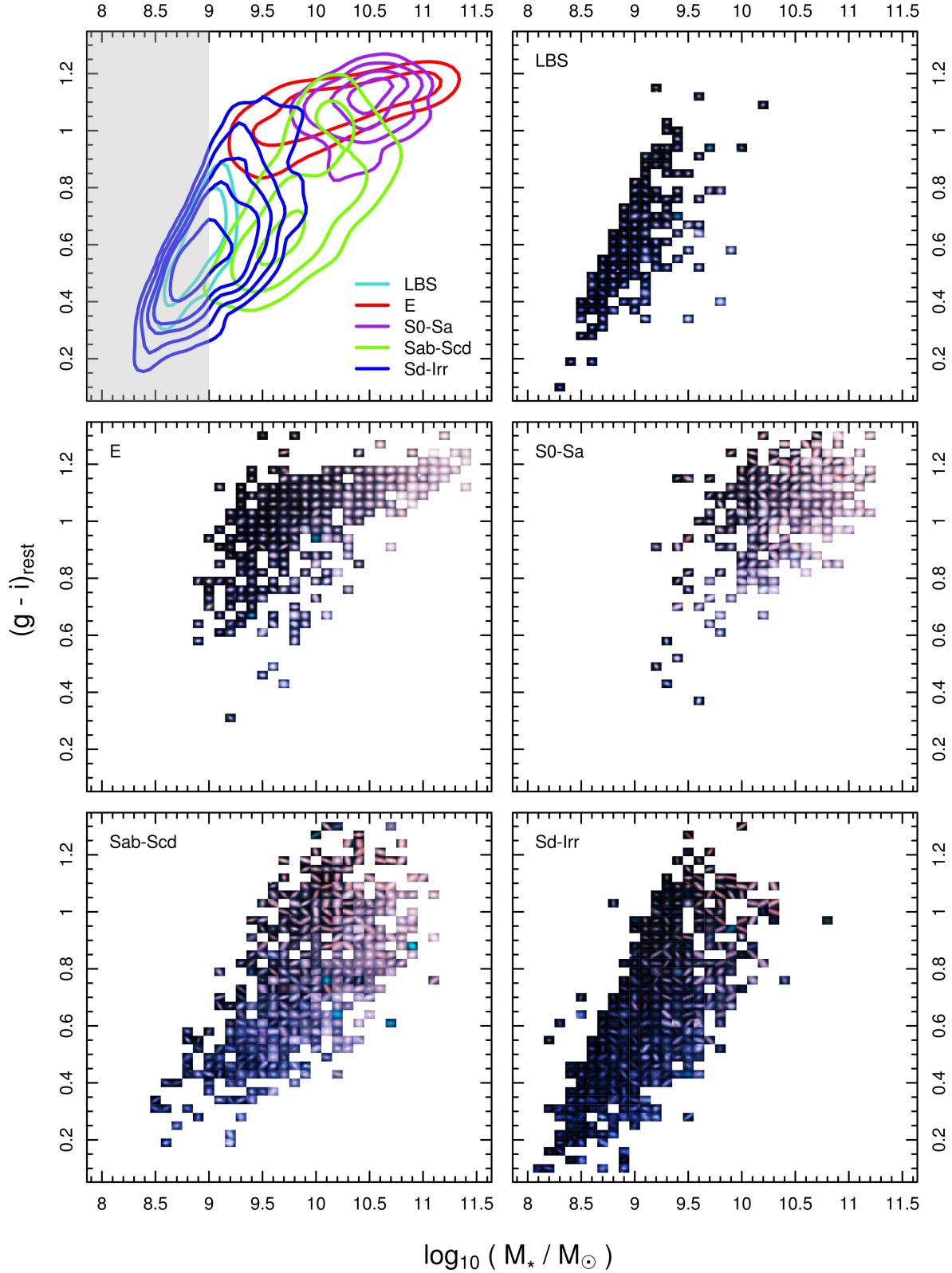
Figure 5. Global rest frame colour, $(g - i)_{\rm rest}$, as a function of $V_{\rm max}$ weight corrected galaxy stellar mass, $\log(\mathcal{M}_*/\mathcal{M}_\odot)$. The top left panel displays several overlaid contour maps highlighting the population density in colour-mass space for each of our morphological types, as indicated by the inset legend. Contours represent 5, 10, 20, 40 and 80% of the peak total population density. The shaded grey area at $\log(\mathcal{M}_*/\mathcal{M}_\odot) < 9.0$ represents the region in which our data becomes stellar mass incomplete. The remaining panels represent a similar colour-mass space but for each population in isolation, as labelled in the top left corner of each panel. For each panel, we display a 3-colour (RGB = Hig) postage stamp image of a galaxy at each position within a grid of bin sizes 0.1 in stellar mass and 0.03 in colour. Each postage stamp is approximately $7'' \times 7''$ in size. Blank spaces indicate a grid element where no galaxy of that morphological class exists.

Visual classification error for the remaining morphological types remains minimal however, typically of the order of or less than the quoted standard errors. We find that our recovered $\mathcal{M}^*$ parameter for our constituent MSMFs decrease systematically from spheroid dominated to disk dominated galaxies; for E, S0-Sa, Sab-Scd and Sd-Irr type galaxies we find $\log(\mathcal{M}^*/\mathcal{M}_\odot) = 10.94, 10.25, 10.09, 9.57$.

Our combined spheroid dominated and disk dominated single Schechter fits provide an excellent description of the spheroid and disk dominated galaxy populations. The goodness of fit estimators both indicate the Schechter model is able to adequately and accurately reproduce the distribution observed in the data, whilst the quoted errors, both standard and visual, remain low. Further, we note that the recovered Schechter fit parameters to our spheroid-dominated and disk-dominated populations: $\log\mathcal{M}^* = 10.60, 10.70$; $\alpha = -0.27, -1.37$, and; $\phi^* = 3.96, 0.98$, respectively, are in good agreement with those found for our double Schechter fit to the total population: $\log\mathcal{M}^* = 10.64, 10.64$; $\alpha = -0.43, -1.50$; $\phi^* = 4.18, 0.74$. The apparent self-similarity between these two sets of recovered parameters supports the notion that our division of the GSMF into spheroid-dominated and disk-dominated sub-populations is indeed physically meaningful. By dividing galaxies according to their dominant structural component, we have been able to naturally recover the fundamental parameters which best describe the full stellar mass distribution of galaxies in the local Universe.

5 CONCLUSIONS

We have analysed a morphologically classified sample of $2,711$ galaxies selected from the GAMA survey by virtue of their redshift range ($0.025 < z < 0.06$) and global stellar mass ($\log(\mathcal{M}_*/\mathcal{M}_\odot) > 9.0$). Each galaxy is classified into either elliptical (E), spheroid-dominated lenticular and early-type spiral (S0-Sa), intermediate/late-type spiral (Sab-Scd) and a disk-dominated or irregular (Sd-Irr) class. Within this local sample, we find approximate stellar mass proportions for E : S0-Sa : Sab-Scd : Sd-Irr of $34 : 37 : 24 : 5$, acknowledging a potential cross-contamination between our elliptical and S0-Sa classes. We find that colour and mass cuts do not trivially recover Hubble type classifications and advocate against using 'red' and 'blue' terminology interchangeably with 'early' and 'late', or 'spheroid dominated' and 'disk dominated' as these are clearly very different distinctions. Grouping by the dominant structural component, spheroid or disk, we further find that approximately $71^{+3}_{-4}\%$ of the stellar mass is currently found within spheroid dominated elliptical and S0-Sa type galaxies, with $29^{+4}_{-3}\%$ residing in disk dominated Sab-Scd and Sd-Irr systems. Adopting reasonable bulge-to-total values (e.g., Graham & Worley 2008) implies that approximately half the stellar mass today resides in spheroidal structures, with the remaining half within disk-like structures, in-line with previous studies (see Driver et al. 2007a,b; Gadotti 2009; Tasca & White 2011).

The total galaxy stellar mass function for our sample is well described by a double Schechter function with parameters $\mathcal{M}^* = 10^{10.64}\mathcal{M}_\odot$, $\alpha_1 = -0.43$, $\phi_1^* = 4.18$ dex^{-1}Mpc^{-3}, $\alpha_2 = -1.50$ and $\phi_2^* = 0.74$ dex^{-1}Mpc^{-3}. The constituent morphological-type stellar mass functions are well sampled above our lower stellar mass limit, with the exception of the little blue spheroid population, which remains incomplete down to $\log(\mathcal{M}_*/\mathcal{M}_\odot) \sim 9.0$. Each morphological-type stellar mass function is adequately described by a single Schechter function (Figure 3), with a notable underestimation of the number density of elliptical galaxies at low stellar masses ($\log(\mathcal{M}_*/\mathcal{M}_\odot) < 10$), and an underestimation of our Sab-Scd population number density at high stellar masses ($\log(\mathcal{M}_*/\mathcal{M}_\odot) \sim 11$). We find our recovered $\mathcal{M}^*$ for these morphological-type stellar mass functions decreases systematically from spheroid dominated to disk dominated galaxies, i.e.; for E, S0-Sa, Sab-Scd and Sd-Irr type galaxies we find $\log(\mathcal{M}^*/\mathcal{M}_\odot) = 10.94, 10.25, 10.09, 9.57$, respectively.

Our combined spheroid dominated and disk dominated stellar mass functions are each well described by a single Schechter function (Figure 4). Interestingly, our recovered $\mathcal{M}^*$ parameters for our combined spheroid dominated and disk dominated stellar mass functions are remarkably similar to one another, in addition to our total galaxy stellar mass function, with $\log(\mathcal{M}^*/\mathcal{M}_\odot) = 10.60$ and 10.70 respectively, as compared with $\log(\mathcal{M}^*/\mathcal{M}_\odot) = 10.64$. We also find a good level of agreement between our spheroid and disk-dominated populations and the total galaxy stellar mass function for the additional Schechter fit parameters, α and ϕ^*. That these two sets of values should arise naturally from the data supports the notion that the combined total galaxy stellar mass function is indeed comprised of two complementary, yet distinct, sub-populations, each best described according to their dominant structural component. We find that the discrepancy between our spheroid dominated stellar mass function and the comparison red sequence stellar mass functions of Baldry et al. (2012) and Peng et al. (2012) at the low mass end of our sample can potentially be attributed to late type contamination of the red sequence (Figure 5), although we note that a division of the local galaxy population by colour may not easily be comparable to a division by dominant structural component; nor should it. In addition, the inclusion of the LBS population into the spheroid dominated class acts to remove the observed low-mass discrepancy, however; it is not clear that this inclusion is desired. Therefore, in conclusion, our campaign of robust morphological classification shows that the local galaxy stellar mass function is adequately described by a double Schechter function comprised of two distinct populations: spheroid dominated and disk dominated galaxies.

$\log\left(\mathcal{M}^*/\mathcal{M}_\odot\right)$	α_1	$\phi_1^*/10^{-3}$ $(\text{dex}^{-1}\text{Mpc}^{-3})$	α_2	$\phi_2^*/10^{-3}$ $(\text{dex}^{-1}\text{Mpc}^{-3})$	χ^2/ν	$\delta_\phi/10^7$ $(\mathcal{M}_\odot\text{Mpc}^{-3})$	$\delta_\Sigma/10^7$ $(\mathcal{M}_\odot\text{Mpc}^{-3})$
10.64 ± 0.07	-0.43 ± 0.35	4.18 ± 1.52	-1.50 ± 0.22	0.74 ± 1.13	1.12	22.07 ± 7.91	$21.88^{+6.90}_{-5.22}$

Table 2. Double Schechter stellar mass function fit parameters for the total GSMF as shown in Figure 3. From left to right, columns are: the shared knee in the Schechter function ($\mathcal{M}^*$); the primary slope of the faint end of the Schechter function (α_1); the primary normalisation constant for the Schechter function (ϕ_1^*); the secondary slope of the faint end of the Schechter function (α_2); the secondary normalisation constant for the Schechter function (ϕ_2^*); the χ^2 goodness of fit parameter (χ^2/ν); the stellar mass density implied in the usual way via the fitted Schechter function [$\rho_\phi = \sum_{i=1}^{N} \phi_i^* \mathcal{M}^* \Gamma\left(\alpha_i + 2\right)$]; the stellar mass density calculated via the direct summation of the stellar masses from the individual galaxies [$\rho_\Sigma = \frac{1}{V}\sum_{i=1}^{N} \mathcal{M}_*$]. The double Schechter function is fit to $N = 24$ data bins with $n = 5$ fitted parameters, therefore, the number of degrees of freedom for this fit is given by $\nu = N - n = 19$.

Population	$\log\left(\mathcal{M}^*/\mathcal{M}_\odot\right)$	α	$\phi^*/10^{-3}$ $(\text{dex}^{-1}\text{Mpc}^{-3})$	χ^2/ν	$\rho_\phi/10^7$ $(\mathcal{M}_\odot\text{Mpc}^{-3})$	$\rho_\Sigma/10^7$ $(\mathcal{M}_\odot\text{Mpc}^{-3})$
E	$10.94 \pm 0.10 \pm 0.18$	$-0.79 \pm 0.13 \pm 0.23$	$0.85 \pm 0.27 \pm 0.49$	3.10	6.81 ± 1.47	$7.46^{+2.40}_{-1.81}$
S0-Sa	$10.25 \pm 0.07 \pm 0.03$	$0.87 \pm 0.23 \pm 0.15$	$2.38 \pm 0.83 \pm 0.27$	1.11	7.53 ± 2.08	$7.98^{+2.51}_{-1.90}$
Sab-Scd	$10.09 \pm 0.15 \pm 0.09$	$-0.01 \pm 0.31 \pm 0.26$	$3.57 \pm 0.81 \pm 0.63$	4.07	4.34 ± 1.62	$5.18^{+1.57}_{-1.20}$
Sd-Irr	$9.57 \pm 0.17 \pm 1.30$	$-1.36 \pm 0.29 \pm 0.80$	$3.40 \pm 2.07 \pm 4.29$	1.66	1.77 ± 1.10	$1.13^{+0.38}_{-0.28}$
Spheroid Dominated	$10.60 \pm 0.05 \pm 0.08$	$-0.27 \pm 0.16 \pm 0.20$	$3.96 \pm 1.05 \pm 0.37$	1.59	14.49 ± 3.92	$15.44^{+4.91}_{-3.71}$
Disk Dominated	$10.70 \pm 0.23 \pm 0.07$	$-1.37 \pm 0.11 \pm 0.04$	$0.98 \pm 0.42 \pm 0.14$	0.90	7.08 ± 3.91	$6.31^{+1.95}_{-1.48}$

Table 3. As Table 2, but single Schechter stellar mass function fit parameters for the Morphological-Type Stellar Mass Functions (MSMFs) in Figures 3 and 4. The second set of confidence intervals for the $\log\mathcal{M}^*$, α and ϕ^* parameters indicate one standard deviation as determined from single-Schechter fits to each individual observers data sets. These single Schechter functions are fit to $N = 24$ data bins with $n = 3$ fitted parameters, therefore, the number of degrees of freedom for this fit is given by $\nu = N - n = 21$.

and the participating institutions. The GAMA website is http://www.gama-survey.org/.

References

Abazajian K. N. et al., 2009, ApJS, 182, 543
Allen P. D., Driver S. P., Graham A. W., Cameron E., Liske J., de Propris R., 2006, MNRAS, 371, 2
Baldry I. K., Balogh M. L., Bower R. G., Glazebrook K., Nichol R. C., Bamford S. P., Budavari T., 2006, MNRAS, 373, 469
Baldry I. K. et al., 2012, MNRAS, 421, 621
Baldry I. K., Glazebrook K., Brinkmann J., Ivezić Ž., Lupton R. H., Nichol R. C., Szalay A. S., 2004, ApJ, 600, 681
Baldry I. K., Glazebrook K., Driver S. P., 2008, MNRAS, 388, 945
Baldry I. K. et al., 2010, MNRAS, 404, 86
Bamford S. P. et al., 2009, MNRAS, 393, 1324
Behroozi P. S., Wechsler R. H., Conroy C., 2013, ApJ, 770, 57
Bell E. F., McIntosh D. H., Katz N., Weinberg M. D., 2003, ApJS, 149, 289
Blanton M. R., Eisenstein D., Hogg D. W., Schlegel D. J., Brinkmann J., 2005, ApJ, 629, 143
Bolzonella M. et al., 2010, A&A, 524, A76
Bruzual G., Charlot S., 2003, MNRAS, 344, 1000

Bundy K. et al., 2010, ApJ, 719, 1969
Calzetti D., Armus L., Bohlin R. C., Kinney A. L., Koornneef J., Storchi-Bergmann T., 2000, ApJ, 533, 682
Cameron E., 2011, PASA, 28, 128
Caon N., Capaccioli M., D'Onofrio M., 1993, MNRAS, 265, 1013
Cappellari M. et al., 2011a, MNRAS, 413, 813
Cappellari M. et al., 2011b, MNRAS, 416, 1680
Cappellari M. et al., 2013, MNRAS, 432, 1862
Chabrier G., 2003, PASP, 115, 763
Conselice C. J., 2006, MNRAS, 373, 1389
Cook M., Evoli C., Barausse E., Granato G. L., Lapi A., 2010, MNRAS, 402, 941
Cook M., Lapi A., Granato G. L., 2009, MNRAS, 397, 534
Cooper M. C. et al., 2012, MNRAS, 419, 3018
Davies R. L., Efstathiou G., Fall S. M., Illingworth G., Schechter P. L., 1983, ApJ, 266, 41
Davies R. L., Illingworth G., 1983, ApJ, 266, 516
De Lucia G., Blaizot J., 2007, MNRAS, 375, 2
De Lucia G., Kauffmann G., White S. D. M., 2004, MNRAS, 349, 1101
Debattista V. P., Mayer L., Carollo C. M., Moore B., Wadsley J., Quinn T., 2006, ApJ, 645, 209
D'Onofrio M., Zaggia S. R., Longo G., Caon N., Capaccioli M., 1995, A&A, 296, 319
Driver S. P. et al., 2006, MNRAS, 368, 414
Driver S. P., Allen P. D., Liske J., Graham A. W., 2007a, ApJ, 657, L85

Driver S. P. et al., 2011, MNRAS, 413, 971

Driver S. P., Liske J., Cross N. J. G., De Propris R., Allen P. D., 2005, MNRAS, 360, 81

Driver S. P. et al., 2009, Astronomy and Geophysics, 50, 050000

Driver S. P., Popescu C. C., Tuffs R. J., Liske J., Graham A. W., Allen P. D., de Propris R., 2007b, MNRAS, 379, 1022

Driver S. P., Robotham A. S. G., Bland-Hawthorn J., Brown M., Hopkins A., Liske J., Phillipps S., Wilkins S., 2013, MNRAS, 430, 2622

Duc P.-A. et al., 2011, MNRAS, 417, 863

Emsellem E. et al., 2011, MNRAS, 414, 888

Gadotti D. A., 2009, MNRAS, 393, 1531

Graham A. W., Colless M. M., Busarello G., Zaggia S., Longo G., 1998, A&AS, 133, 325

Graham A. W., Driver S. P., 2005, PASA, 22, 118

Graham A. W., Merritt D., Moore B., Diemand J., Terzić B., 2006, AJ, 132, 2711

Graham A. W., Worley C. C., 2008, MNRAS, 388, 1708

Hill D. T. et al., 2011, MNRAS, 412, 765

Kauffmann G. et al., 2003, MNRAS, 341, 54

Kauffmann G., White S. D. M., Heckman T. M., Ménard B., Brinchmann J., Charlot S., Tremonti C., Brinkmann J., 2004, MNRAS, 353, 713

Kelvin L., Driver S., Robotham A., Hill D., Cameron E., 2010, in American Institute of Physics Conference Series, Vol. 1240, American Institute of Physics Conference Series, Debattista V. P., Popescu C. C., eds., pp. 247–248

Kelvin L. S. et al., 2014, MNRAS, 439, 1245

Kelvin L. S. et al., 2012, MNRAS, 421, 1007

Kereš D., Katz N., Weinberg D. H., Davé R., 2005, MNRAS, 363, 2

Khochfar S. et al., 2011, MNRAS, 417, 845

Khochfar S., Silk J., 2006a, ApJ, 648, L21

Khochfar S., Silk J., 2006b, MNRAS, 370, 902

Kormendy J., Bender R., 2012, ApJS, 198, 2

Krajnović D. et al., 2011, MNRAS, 414, 2923

Lara-López M. A. et al., 2010, A&A, 521, L53

Lara-López M. A. et al., 2013, MNRAS, 434, 451

Lawrence A. et al., 2007, MNRAS, 379, 1599

L'Huillier B., Combes F., Semelin B., 2012, A&A, 544, A68

Liske J., Lemon D. J., Driver S. P., Cross N. J. G., Couch W. J., 2003, MNRAS, 344, 307

Matković A., Guzmán R., 2005, MNRAS, 362, 289

Moustakas J. et al., 2013, ApJ, 767, 50

Muzzin A. et al., 2013, ApJ, 777, 18

Navarro J. F., Benz W., 1991, ApJ, 380, 320

Omand C., Balogh M., Poggianti B., 2014, arXiv:1402.3394

Pastrav B. A., Popescu C. C., Tuffs R. J., Sansom A. E., 2013, A&A, 553, A80

Patel S. G. et al., 2013, ApJ, 766, 15

Peng C. Y., Ho L. C., Impey C. D., Rix H.-W., 2002, AJ, 124, 266

Peng C. Y., Ho L. C., Impey C. D., Rix H.-W., 2010a, AJ, 139, 2097

Peng Y.-j. et al., 2010b, ApJ, 721, 193

Peng Y.-j., Lilly S. J., Renzini A., Carollo M., 2012, ApJ, 757, 4

Pichon C., Pogosyan D., Kimm T., Slyz A., Devriendt J., Dubois Y., 2011, MNRAS, 418, 2493

Pozzetti L. et al., 2010, A&A, 523, A13

Robotham A. S. G. et al., 2013, MNRAS, 431, 167

Robotham A. S. G. et al., 2011, MNRAS, 416, 2640

Schechter P., 1976, ApJ, 203, 297

Schmidt M., 1968, ApJ, 151, 393

Sérsic J. L., 1963, Boletin de la Asociacion Argentina de Astronomia La Plata Argentina, 6, 41

Shankar F., Marulli F., Bernardi M., Mei S., Meert A., Vikram V., 2013, MNRAS, 428, 109

Shen S., Mo H. J., White S. D. M., Blanton M. R., Kauffmann G., Voges W., Brinkmann J., Csabai I., 2003, MNRAS, 343, 978

Shimizu I., Inoue A. K., 2013, arXiv:1310.0879

Simard L., Mendel J. T., Patton D. R., Ellison S. L., McConnachie A. W., 2011, ApJS, 196, 11

Szomoru D., Franx M., van Dokkum P. G., Trenti M., Illingworth G. D., Labbé I., Oesch P., 2013, ApJ, 763, 73

Tasca L. A. M., White S. D. M., 2011, A&A, 530, A106

Taylor E. N. et al., 2011, MNRAS, 418, 1587

Tomczak A. R. et al., 2014, ApJ, 783, 85

Tremonti C. A. et al., 2004, ApJ, 613, 898

van den Bosch F. C., Aquino D., Yang X., Mo H. J., Pasquali A., McIntosh D. H., Weinmann S. M., Kang X., 2008, MNRAS, 387, 79

van Dokkum P. G. et al., 2010, ApJ, 709, 1018

White S. D. M., Frenk C. S., 1991, ApJ, 379, 52

Wyse R. F. G., Gilmore G., Franx M., 1997, ARA&A, 35, 637

Yang X., Mo H. J., van den Bosch F. C., 2009, ApJ, 695, 900

York D. G. et al., 2000, AJ, 120, 1579

Young C. K., Currie M. J., 1994, MNRAS, 268, L11

APPENDIX A: IMPACT OF THE LBS POPULATION ON THE GSMF

Our prior division of our galaxy sample into spheroid dominated (E, S0-Sa) and disk dominated (Sab-Scd, Sd-Irr) galaxies, as shown in Figure 4, neglected the low-mass little blue spheroid population. Figure A1 shows the GSMF and disk dominated MSMF as before, but with an updated spheroid dominated MSMF including the LBS population (i.e., E, S0-Sa, LBS). All data analysis is conducted in a similar fashion to that outlined in Section 4. The previous spheroid dominated (E, S0-Sa) single Schechter function fit is shown in light grey, for reference. As can clearly be seen, once the LBS galaxy population is included into the spheroid dominated class, we recover a low-mass upturn exceedingly similar in nature to the red population as reported in, e.g., Baldry et al. (2012) and Peng et al. (2012). On the surface, the spheroid dominated class may perhaps be the natural home of the 'little blue spheroid' galaxy population, allowing us to maintain a good level of agreement with comparison studies.

However, we remind the reader that our adopted visual morphological classification boundaries (Kelvin et al. 2014) are substantially different from the red/blue divisions presented in Baldry et al. (2012) and Peng et al. (2012), and also the star forming/quiescent divisions as noted in Section 4.2. See, for example, Figure 5 for a visual representation of the colour mix across all morphologies. Indeed,

despite the inherent trends between morphology, colour and star formation rate, we see no explicit reason why a bimodal division along morphological lines should reproduce exactly that of one which has been created along colour or star formation rate measures. In which case, it is perhaps surprising that a combined spheroid dominated plus LBS population so closely recovers the low-mass upturn observed in the red populations of Baldry et al. (2012) and Peng et al. (2012). Also note that whilst the third word in LBS denotes its shape, the second part of the acronym denotes their typical colour: blue. As is shown in Figure 5, the majority of blue galaxies lie in the disk dominated Sab-Scd and Sd-Irr classes, giving weight to the inclusion of the LBS population in our disk dominated sub-sample instead. This would only serve to increase the low-mass upturn of the disk dominated population, and maintain the low-mass discrepancy we observe between our spheroid dominated class and the comparison red-population data from the literature. The correct placement of our LBS galaxy population within the morphological schema adopted throughout this study remains unclear, and therefore, we continue to advocate its exclusion at present. Future studies are planned to clarify the importance of the LBS population (Moffett et al., in prep.).

Table A1 provides the double Schechter fit parameters to the combined spheroid dominated (E, S0-Sa) plus LBS population. Note the unusually low α_2 slope parameter, combined with relatively large error bars. This indicates that shape of the low-mass end of our Schechter fit is poorly constrained, as is evidenced by the unusually steep gradient of the fit when extrapolated below our mass limit (see Figure A1). Nevertheless, the Schechter fit provides a good description of the data across the range of interest $(\log(\mathcal{M}_*/\mathcal{M}_\odot) > 9.0)$, exhibiting a strong goodness of fit parameter.
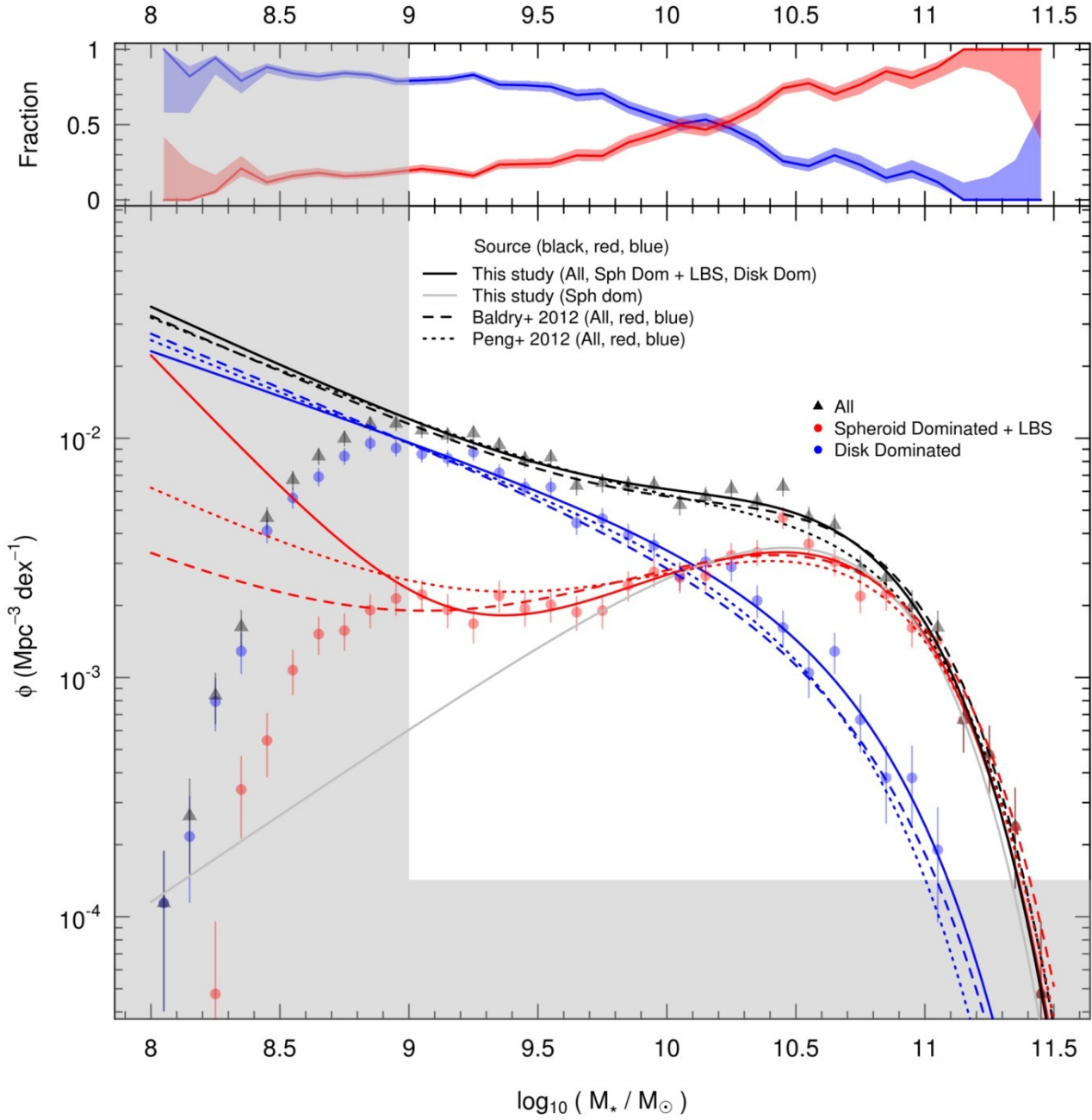
Figure A1. As Figure 4, but with the inclusion of the LBS population in the spheroid dominated class (red data points). The combined spheroid dominated plus LBS population is fitted by a double Schechter component (red solid line) as is the total galaxy population (solid black line), whereas the disk dominated population remains well described by a single Schechter function (solid blue line). The previous spheroid dominated (E, S0-Sa) single Schechter function fit is shown in light grey, for reference. Comparison Schechter function fits for similar red and blue populations from Baldry et al. (2012) and Peng et al. (2012) are also shown.

$\log\left(\mathcal{M}^*/\mathcal{M}_\odot\right)$	α_1	$\phi_1^*/10^{-3}$ $(\mathrm{dex}^{-1}\mathrm{Mpc}^{-3})$	α_2	$\phi_2^*/10^{-3}$ $(\mathrm{dex}^{-1}\mathrm{Mpc}^{-3})$	χ^2/ν	$\delta_\phi/10^7$ $(\mathcal{M}_\odot\mathrm{Mpc}^{-3})$	$\delta_\Sigma/10^7$ $(\mathcal{M}_\odot\mathrm{Mpc}^{-3})$
10.65 ± 0.08	-0.37 ± 0.23	3.63 ± 1.38	-2.13 ± 1.23	0.01 ± 0.05	0.96	14.29 ± 7.76	$15.56^{+4.95}_{-3.74}$

Table A1. Double Schechter stellar mass function fit parameters for the combined spheroid dominated plus LBS galaxy population as shown in Figure A1. From left to right, columns are: the shared knee in the Schechter function ($\mathcal{M}^*$); the primary slope of the faint end of the Schechter function (α_1); the primary normalisation constant for the Schechter function fit (ϕ_1^*); the secondary slope of the faint end of the Schechter function (α_2); the secondary normalisation constant for the Schechter function fit (ϕ_2^*); the χ^2 goodness of fit parameter (χ^2/ν); the stellar mass density implied in the usual way via the fitted Schechter function [$\rho_\phi = \sum_{i=1}^{N} \phi_i^* \mathcal{M}^* \Gamma\left(\alpha_i + 2\right)$]; the stellar mass density calculated via the direct summation of the stellar masses from the individual galaxies [$\rho_\Sigma = \frac{1}{V}\sum_{i=1}^{N}\mathcal{M}_*$]. The double Schechter function is fit to $N = 24$ data bins with $n = 5$ fitted parameters, therefore, the number of degrees of freedom for this fit is given by $\nu = N - n = 19$.